ARTICLES
PUBLISHED ONLINE: 12 OCTOBER 2015 | DOI: 10.1038/NMAT4444
nature materials

Cell-mediated fibre recruitment drives extracellular matrix mechanosensing in engineered fibrillar microenvironments

Brendon M. Baker[1,2*†], Britta Trappmann[1,2†], William Y. Wang[1], Mahmut S. Sakar[3], Iris L. Kim[4], Vivek B. Shenoy[5], Jason A. Burdick[4] and Christopher S. Chen[1,2*]

To investigate how cells sense stiffness in settings structurally similar to native extracellular matrices, we designed a synthetic fibrous material with tunable mechanics and user-defined architecture. In contrast to flat hydrogel surfaces, these fibrous materials recapitulated cell–matrix interactions observed with collagen matrices including stellate cell morphologies, cell-mediated realignment of fibres, and bulk contraction of the material. Increasing the stiffness of flat hydrogel surfaces induced mesenchymal stem cell spreading and proliferation; however, increasing fibre stiffness instead suppressed spreading and proliferation for certain network architectures. Lower fibre stiffness permitted active cellular forces to recruit nearby fibres, dynamically increasing ligand density at the cell surface and promoting the formation of focal adhesions and related signalling. These studies demonstrate a departure from the well-described relationship between material stiffness and spreading established with hydrogel surfaces, and introduce fibre recruitment as a previously undescribed mechanism by which cells probe and respond to mechanics in fibrillar matrices.

The adhesion of cells to the extracellular matrix (ECM) regulates many cellular functions including spreading, migration, proliferation and differentiation, and thus plays a major role in embryonic development, adult tissue homeostasis and disease pathogenesis[1–3]. As the biophysical and biochemical properties of native ECMs are difficult to experimentally modulate, synthetic materials have been crucial towards isolating the contributions of specific matrix properties in regulating cell adhesion and function. In particular, elastic hydrogel surfaces (for example, polyacrylamide gels) have proved indispensable in demonstrating that substrate stiffness or rigidity can itself modulate cell behaviour[4–6], as these materials afford precise control of stiffness, independent of cell-adhesive ligand density[7]. However, it is unclear how findings on these smooth, flat surfaces extend to *in vivo* settings, where cells reside in or on complex three-dimensional (3D) ECMs consisting of meshworks of fibres with diameters typically of the order of micrometres[8–10]. These networks of fibres vary widely in density and organization depending on the tissue (for example, dense, aligned collagen bundles in tendon versus loose, less organized networks in glandular organs). The micrometre-scale architecture of these fibrous networks constrains spatially where cells can form adhesions and imparts complex mechanical characteristics due to nonlinear stiffening in response to loading and differential rigidity in axial versus transverse directions with respect to fibre orientation—all features that cannot be captured with existing isotropic, linear elastic hydrogel surfaces. Given the lack of mechanically tunable synthetic materials possessing fibrous structure at physiologic length scales, an understanding of how cells sense and respond to the mechanics of fibrillar microenvironments remains an open challenge. Here, we establish a new material system that incorporates fibrillar structure while still maintaining synthetic control over mechanical and adhesive features and apply this system to elucidate mechanisms of how cells interpret ECM stiffness in fibrous networks.

Fibrillar ECM with controllable architecture and mechanics

To develop a material system for studying fibrillar mechanosensing, we combined polymer chemistry, electrospinning and soft lithography. As a base material, we formulated a protein-resistant, methacrylated dextran[11] (DexMA, Fig. 1a and Supplementary Fig. 1) that could be functionalized with cell-adhesive moieties following substrate fabrication (Fig. 1a and Supplementary Figs 3 and 4). Fibre networks with controllable architecture and mechanics were fabricated by electrospinning the polymer onto collection substrates such that fibres were suspended across microfabricated wells. The geometry of the wells defined boundary conditions and elevated networks to exclude a mechanical contribution from the underlying rigid surface. Numerous structural parameters were tuned in this system, including fibre diameter (through solution concentration, Supplementary Fig. 7), fibre density (through fibre collection durations) and fibre anisotropy (through rotational speed of the collection surface; Fig. 1b). Exposure to ultraviolet light crosslinked DexMA, rendering fibres insoluble and allowing stiffness to be modulated through the extent of light exposure. To measure the mechanics of individual DexMA fibres as a function of ultraviolet light exposure, we performed microscale

[1]Tissue Microfabrication Lab, Department of Biomedical Engineering, Boston University, Boston, Massachusetts 02215, USA. [2]Wyss Institute for Biologically Inspired Engineering, Center for Life Science Boston Building, 5th Floor, 3 Blackfan Circle, Boston, Massachusetts 02115, USA. [3]Institute of Robotics and Intelligent Systems, Eidgenössische Technische Hochschule Zürich, CH-8092 Zürich, Switzerland. [4]Department of Bioengineering, University of Pennsylvania, Philadelphia, Pennsylvania 19104, USA. [5]Department of Materials Science and Engineering, University of Pennsylvania, Philadelphia, Pennsylvania 19104, USA. †These authors contributed equally to this work. *e-mail: bambren@bu.edu; chencs@bu.edu

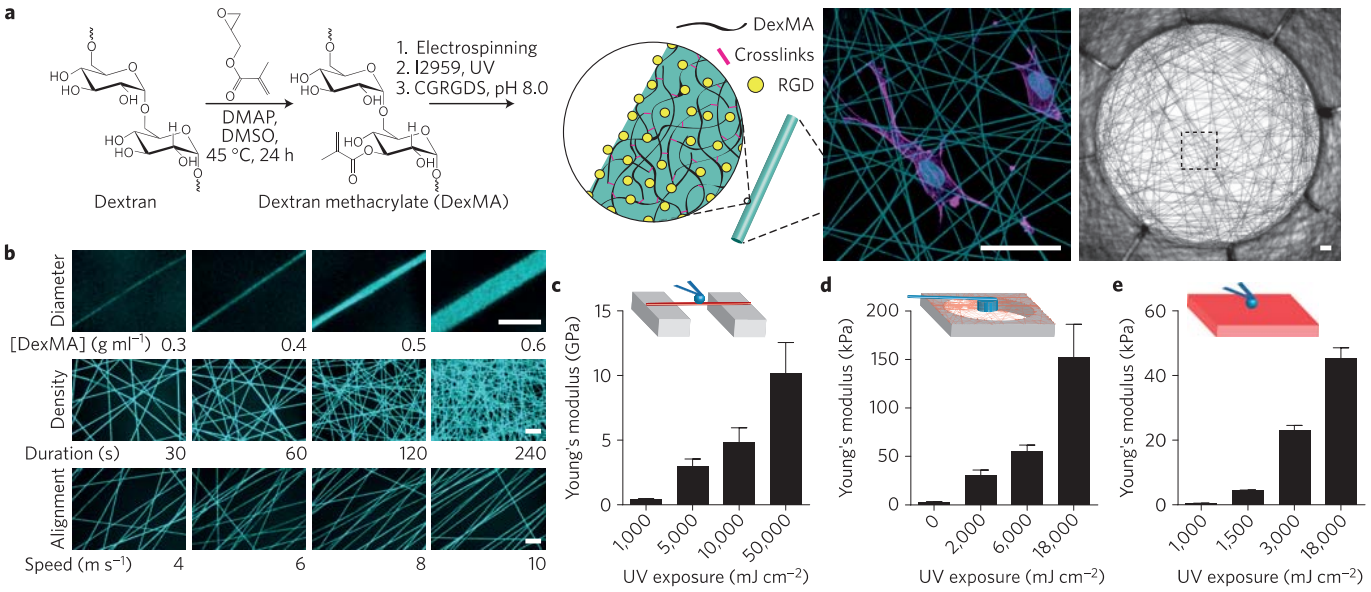

Figure 1 | A new approach to engineering fibrillar microenvironments with tunable mechanical and architectural features. a, Hierarchical overview of fabricating cell-adhesive suspended networks of DexMA fibres. Dextran is reacted with glycidyl methacrylate to generate DexMA. Following addition of a photoinitiator, DexMA is electrospun onto microfabricated substrates to define networks of suspended fibres. Networks are photocrosslinked to tune fibre stiffness and the RGD is incorporated to enable cell attachment. Scale bars, 100 μm. **b**, Through modulation of the electrospinning fabrication process, networks with varying fibre diameter (polymer solution concentration), density (fibre collection duration) and alignment (collection surface translation speed) can be generated, enabling the modelling of diverse fibrillar ECMs present in different tissue systems throughout the body. Scale bars, 10 μm. **c**, Young's modulus of individual fibres isolated over PDMS troughs and measured by three-point bending AFM; $n \geq 12$, mean ± s.d. **d**, Young's modulus of DexMA fibre networks measured by cylindrical indentation with a calibrated cantilever; $n \geq 5$, mean ± s.d. **e**, Young's modulus of DexMA flat hydrogels determined by AFM spherical probe nanoindentation and Hertz contact mechanics; $n \geq 6$, mean ± s.d.

three-point bending tests using atomic force microscopy[12,13] (AFM; Supplementary Fig. 2). Young's modulus of individual fibres was tunable between 140 MPa and 10 GPa (Fig. 1c), approximating the range of reported values for various fibrous biopolymers such as collagen (0.5–10 GPa; refs 12,14). As cells probe the mechanics of not just a single fibre, but a network composed of many fibres, a macroscale measurement of network mechanics was also developed (Supplementary Fig. 2). Increasing ultraviolet light exposure to increase fibre modulus without altering other network parameters (Supplementary Figs 3 and 9) led to an increase in network stiffness as expected (Fig. 1d). A salient feature of the DexMA polymer is that in addition to fibrous networks, we can generate smooth hydrogel surfaces lacking fibrous topography from the same material to serve as a direct comparator in our studies. Tuning mechanics by photocrosslinking yielded hydrogels with moduli between 450 Pa and 45 kPa as determined by AFM nanoindentation and Hertz contact mechanics (Fig. 1e).

On processing DexMA into hydrogel or fibrillar form, the adhesive peptide CGRGDS (RGD) was coupled to substrates through Michael-type addition with unreacted methacrylates (Supplementary Figs 3 and 4). Although functionalization with other peptides or even full-length proteins is possible, we chose a non-fibrillar adhesion moiety to exclude the confounding mechanical contribution of a superimposed meshwork of ECM proteins, which has previously been shown to influence cellular mechanosensing[15]. Thus, RGD coupled directly to DexMA fibre networks or hydrogel surfaces ensured that the ECM stiffness experienced by seeded cells was defined entirely by the structure of the material.

Synthetic fibre networks mimic collagen matrices

Several distinctions exist between this material and *in vivo* ECMs or even purified fibrous biopolymers such as type I collagen. Structural features including persistence length, tortuosity, fibre diameter and 3D organization are likely to diverge from natural fibrillar ECMs. Biochemically, the exclusive use of RGD differs from the more complex ligand–receptor interactions mediating adhesion to native fibrillar proteins, such as the additional GFOGER and GVMGFO adhesion sequences on collagens or tension-induced exposure of cryptic binding sites in fibronectin[16–19]. Given these disparities, we assessed how faithfully our synthetic fibrillar material recapitulated topographical and mechanical interactions between cells and a bona fide fibrous ECM. For these studies, we chose type I collagen, the most abundant fibrillar protein in mammals and a well-studied model in mechanobiology over several decades[8,20]. As a comparator possessing chemistry identical to fibre networks but lacking fibrous topography, cells were also cultured on the surface of DexMA hydrogels.

We began by examining cytoskeletal organization in cells cultured on these materials. All studies presented here used human mesenchymal stem cells (hMSCs), a model cell type for mechanosensing studies[6,15,21,22], although similar trends were observed with human dermal fibroblasts. A high degree of similarity was observed between DexMA fibre networks and type I collagen matrices (Fig. 2a); cells in both conditions adopted a spindly morphology possessing thin, elongated processes that terminated in branched protrusions, with punctate vinculin-rich focal adhesions (FAs) sequestered to the tips of these protrusions. Centrally located FAs were not visible owing to high cytosolic signal, and hMSCs possessed relatively few actin stress fibres traversing the cytoplasm, although actin was enriched at the hulls of processes. This shift in vinculin from FAs to the cytosol and paucity of stress fibres has been suggested to be representative of cells in 3D matrices or *in vivo* tissues[20,23–26]. In contrast, cells seeded on stiff hydrogels adopted a well-spread, lamellar morphology with larger, elongated FAs distributed throughout the cell and numerous stress fibres similar to cells cultured on

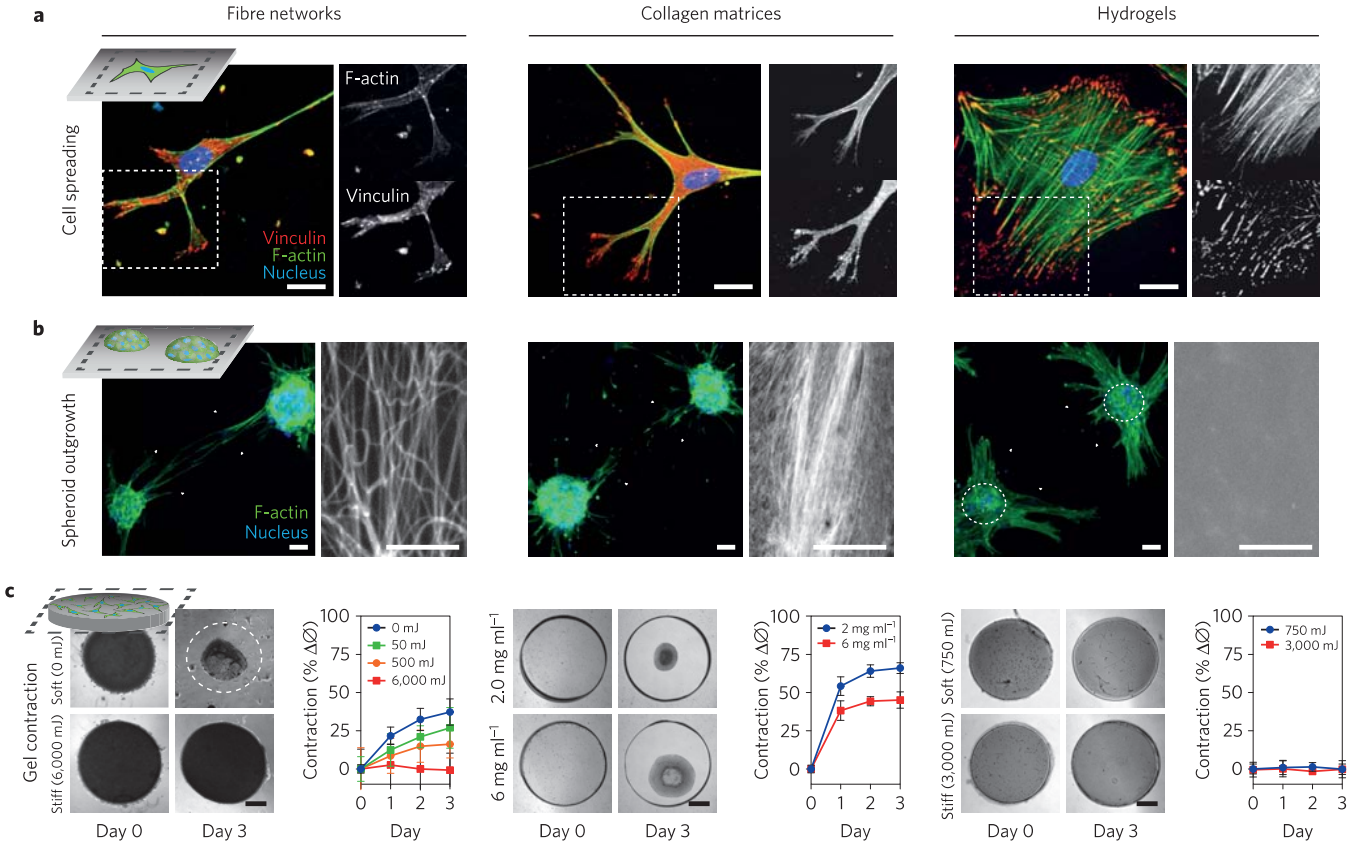

Figure 2 | Synthetic fibre networks induce similar topographical and mechanical interactions with cells to collagen matrices at multiple length scales. **a–c**, Comparison of cell spreading (**a**), spheroid outgrowth (**b**) and gel contraction (**c**) across hMSC-seeded DexMA fibre networks (left column), type I collagen matrices (middle column) and flat DexMA hydrogels (right column). **a**, Cytosolic and focal adhesion-localized vinculin (red), counter-stained for F-actin (green) and cell nuclei (blue) with phalloidin and Hoechst 33342, respectively. Dashed rectangle designates region shown with F-actin or vinculin channel isolated. Scale bars, 50 μm. **b**, Outgrowth of hMSC spheroids (100 cells per spheroid) stained for F-actin (green) and cell nuclei (blue). Rhodamine methacrylate-coupled DexMA fibres and hydrogel surface and Picrosirius red-stained collagen are shown in the region spanning two spheroids, as indicated by the dashed rectangle. Scale bars, 50 μm. **c**, DexMA fibres and hydrogels and collagen were processed into thick circular slabs and seeded at high density with hMSCs. Initial and final states of soft (top) and stiff (bottom) constructs. Cell-mediated contraction was determined by normalizing construct diameter to the initial diameter; mean ± s.d., $n \geq 6$. Scale bars, 500 μm.

glass or plastic[24]. Taken together, the surprising similarity between type I collagen matrices and fibre networks in contrast to flat hydrogel surfaces suggests that fibrillar topography had a stronger influence on cell morphology than the biochemical nature of these interactions.

A historic demonstration of how cellular forces could physically reorganize ECM involved culturing contractile tissue explants within collagen matrices and observing the fibre alignment and directed cell migration in fields of high tension between adjacent explants[27]. To test whether DexMA fibre networks could capture this phenomenon, multicellular hMSC spheroids were seeded on the synthetic fibre networks. Indeed, cell forces pulled fibres into alignment and cells began to directionally migrate towards adjacent spheroids (Fig. 2b), mimicking the response on collagen matrices. This response did not occur on DexMA hydrogels of a range of different stiffnesses, highlighting the comparatively limited range of deformations in non-fibrous materials[28]. These results reinforce a high degree of mechanical similarity between our synthetic fibrillar ECM and collagen, and provide evidence of the potential for ECM remodelling and long-range force transmission in this material[29,30], a process relevant to, for example, cancer cell escape from primary tumours during metastasis[31].

In addition to local remodelling, macroscale contraction has been observed in fibroblast-populated collagen matrices and used to assess how tensile forces generated by cells elicit morphogenetic changes[32–34]. When we seeded DexMA fibre networks unattached to any boundary constraints, compaction occurred over a three-day time course, comparable to collagen (Supplementary Fig. 5), whereas seeded DexMA hydrogels of a range of stiffnesses and unseeded DexMA fibre samples did not change in diameter (Fig. 2c). Altering the concentration of collagen can tune the contraction response over a limited range, but such perturbation simultaneously alters fibril and adhesive ligand density as well as mechanics. Importantly, in contrast to biologic ECMs, we can independently tune fibre stiffness, density and architecture to dictate the ability of cells to deform the material.

Stiff fibres suppress cell spreading and proliferation

Having validated our synthetic material, we next tested whether cells respond to an increase in material stiffness in fibre networks in a similar fashion to hydrogel surfaces. To assay a cell response thoroughly described in the literature, we first examined the relationship between material stiffness and cell spreading. Tuning DexMA crosslinking to define soft (290 Pa) and stiff (19.1 kPa) hydrogels, we confirmed previous observations[4–6,35]: at low stiffness cells failed to spread; with increasing stiffness, spreading and the formation of large lamellae occurred (Fig. 3a–c). To examine a longer term, functional outcome, we measured cell proliferation over a two-day time course. In these experiments, we observed uniformly low cell

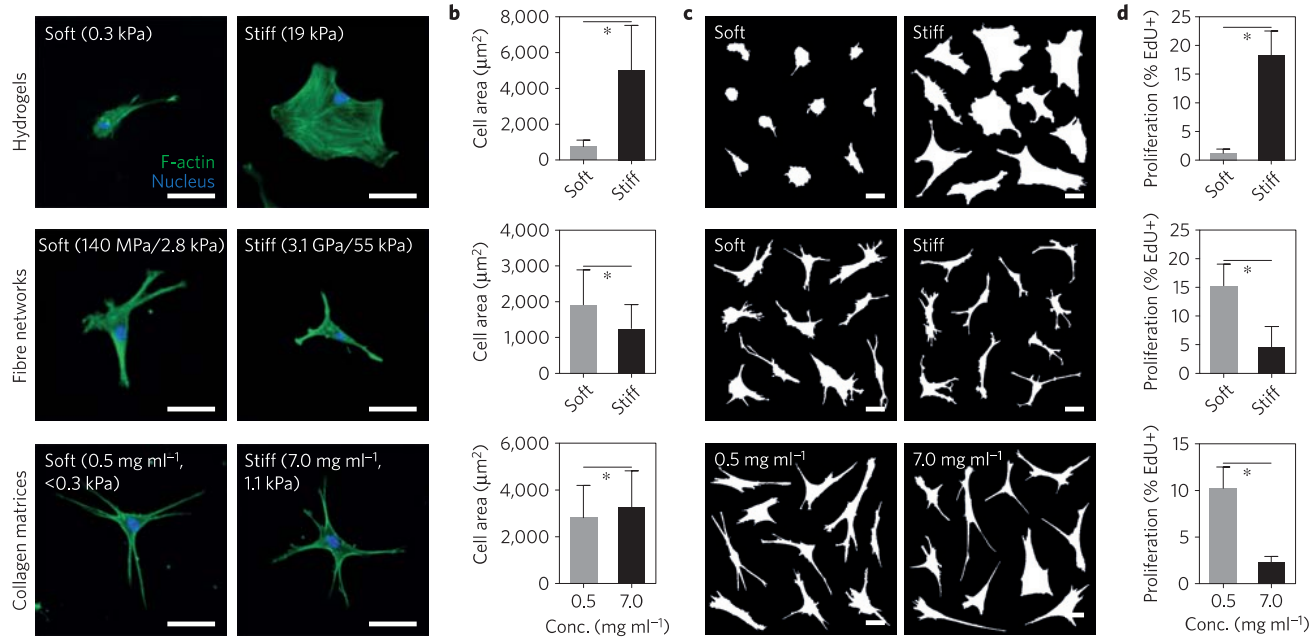

Figure 3 | Increasing fibre stiffness suppresses cell spreading and proliferation. The effect of altering material stiffness on hMSC spreading and proliferation was examined on DexMA hydrogels (top row, soft: 290 Pa, stiff: 19.1 kPa) and fibre networks (middle row, soft: 140 MPa fibre, 2.8 kPa network; stiff: 3.1 GPa fibre, 55 kPa network). Low (0.5 mg ml^{-1}, <0.3 kPa) and high (7.0 mg ml^{-1}, 1.1 kPa) concentration type I collagen matrices where bulk stiffness and adhesive ligand density increase in tandem were included for comparison (bottom row). **a**, Actin cytoskeletal organization of representative hMSCs 16 h after seeding, stained for F-actin (green) and cell nuclei (blue). Scale bars, 50 μm. **b**, Quantification of cell area; mean ± s.d., $n \geq 64$ cells, $^*P < 0.05$. **c**, Cell outlines of ten representative cells. Scale bars, 50 μm. **d**, Proliferation of hMSCs over two days as determined by EdU incorporation; mean ± s.d., $n \geq 13$ regions of interest (ROI) with totals of 750–1,500 cells analysed, $^*P < 0.05$.

death across all conditions, suggesting cytocompatibility and no direct effects of stiffness on cell viability (Supplementary Fig. 8). With stiffness-induced increases in cell area from soft to stiff hydrogels, we observed a commensurate increase in cell proliferation (Fig. 3d), again in line with numerous previous reports[35–37]. Surprisingly, when cells were cultured on soft (fibre: 140 MPa, network: 2.8 kPa) and stiff (fibre: 3.1 GPa, network: 55 kPa) fibre networks with all other parameters maintained constant, cell area did not increase with fibre stiffness as observed on hydrogel surfaces, but instead showed a modest but significant decrease (Fig. 3a–c). Moreover, in stark contrast to hydrogel surfaces, cell proliferation in soft networks was threefold higher than in stiff networks fabricated at the same fibre density (Fig. 3d).

We then examined whether this inverted proliferation response occurs in an established fibrillar setting and excluded an RGD-specific response by repeating the experiment with collagen matrices, in which stiffness and ligand density were simultaneously modulated by altering collagen concentration. Although increasing either stiffness or ligand density alone increases cell area and proliferation on synthetic hydrogels[7,35–38], we found that the soft, low-concentration collagen matrices promoted proliferation relative to stiffer, high-concentration collagen matrices (Fig. 3a–d). Taken together, these data suggest that in fibrous ECMs, the relationship between substratum stiffness and cell function is inverted as compared with on hydrogel surfaces.

Fibre recruitment increases local adhesive ligand density

Modulating fibre stiffness had a significant effect on the ability of cells to reorganize fibres. In soft networks, cells pulled and deformed the networks, resulting in significant recruitment of fibres to the cell and the formation of numerous densely compacted clusters of fibres (Fig. 4a and Supplementary Movie 3). Conversely, stiff networks presented a rigid and essentially immobile ECM that underwent negligible architectural remodelling. The range of deformations in soft networks is illustrated by the displacement of fluorescent microspheres embedded within soft DexMA fibres following cell attachment (Fig. 4b), and qualitatively by movies of cells migrating on soft versus stiff fibres (Supplementary Movies 1 and 2). Microsphere (and fibre) motion was unidirectional and displacements were high in soft networks (Supplementary Fig. 6 and Supplementary Movies 4 and 5). In contrast, displacements in soft hydrogels were an order of magnitude smaller and underwent cyclic motions, suggestive of 'load-and-fail' dynamics described previously[39].

The considerable physical reorganization and clustering of fibres in soft networks resulted in increased adhesive ligand density adjacent to the cell. Time-lapse confocal imaging of fibre networks functionalized with fluorescently tagged RGD demonstrated a rapid 2–3-fold increase of local RGD density following cell attachment to soft networks, with little change in stiff networks (Fig. 4c–d and Supplementary Movie 3). Consistent with the conclusion that increased matrix contact with cells due to fibre recruitment provides the mechanism for enhanced response, we observed that differences in proliferation between soft and stiff fibres decreased and ultimately were eliminated by increasing the initial fibre density of the network (Supplementary Fig. 10). Interestingly, we also observed decreased fibre recruitment with increasing fibre density, possibly due to the distribution of cellular contractile work across more focal adhesions—a phenomenon that has previously been described[40]—deforming each fibre to a lesser degree.

Increases in ligand density could enhance FA assembly[38,41]. Indeed, soft networks were found to promote FA formation (vinculin localization) over stiff networks (Fig. 5b), even when restricting analysis to cells with similar spread areas (as spreading is correlated with enhanced FA formation[4,42]; Fig. 5c). In both conditions FAs localized to the tips of extended cell processes; however, hMSCs on soft networks possessed markedly more

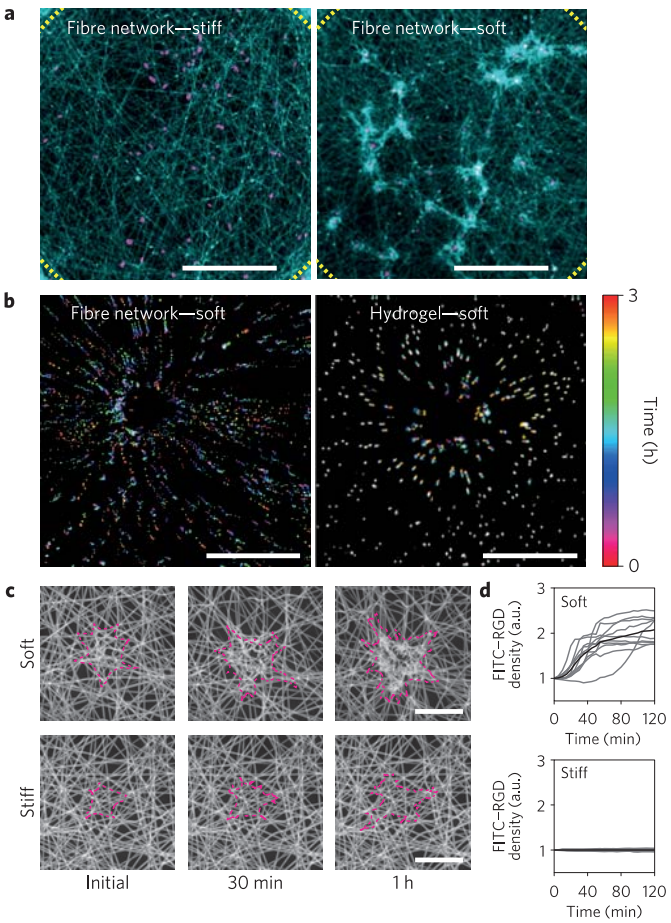

Figure 4 | Lower fibre and network stiffness enables cell-mediated reorganization of the material and clustering of adhesive ligands local to the cell. a, Reorganization of stiff and soft fibre networks 16 h after hMSC seeding. Fibres imaged by coupling with rhodamine methacrylate (cyan) and thresholded cell nuclei labelled with Hoechst 33342 (magenta). Dotted lines indicate the periphery of the suspended network. Scale bars, 500 μm. **b**, Temporally colour-coded overlays capturing the motion of beads embedded within soft fibres (fibre, 140 MPa; network, 2.8 kPa) and soft hydrogels (290 Pa) over a 3 h time course following hMSC seeding. **c**, Time-lapse images of FITC–RGD-coupled fibre recruitment during the first 2 h of hMSCs spreading on soft (top) and stiff (bottom) networks. Cell outlines shown in magenta. Scale bars, 50 μm. **d**, Quantification of FITC–RGD fluorescence intensity in a 50-μm-diameter circular region centred on the cell's nucleus. Intensity was normalized to adjacent acellular areas; $n = 10$ cells.

centrally located FAs, directly localized to underlying clustered fibres. Average FA size, number of FAs and total FA area were all higher in cells on soft fibre networks, and consistently inverted as compared with the response to stiffness on hydrogel surfaces (Fig. 5a,d–f). Focal adhesion kinase (FAK) plays a central role in transducing adhesion into biochemical signals[43], and markedly more phosphorylated FAK was detected at FA sites in soft fibre networks (Fig. 5g–h). This increased FAK activation was functionally important to the proliferation induced on soft networks, as inhibition of FAK with a selective inhibitor (PF-573228; ref. 44) abrogated the increase in proliferation on soft networks (Fig. 5i).

Although these studies implicate an important role for fibre recruitment in the cellular response to fibrous matrices, one alternative explanation for the results is that decreasing fibre stiffness also alters the nanoscale mobility or mechanics of RGD on soft fibres, thereby impacting integrin clustering or catch-bond dynamics[15,39,45,46]. To distinguish fibre recruitment from the effects of RGD mobility or mechanics, we modulated the interconnections or 'welding' between fibres as a means to reduce fibre recruitment without altering the stiffness or RGD mobility of individual fibres (Fig. 5j). In standard networks, fibre intersections were a mixture of welded and unwelded states (Supplementary Movies 6 and 8). To maximize fibre–fibre welding, networks were placed in a controlled humidity environment and provided sufficient moisture before light exposure to fuse all juxtaposed fibres (Fig. 5j and Supplementary Movie 7). Indeed, this welding resulted in reduced fibre clustering compared with soft networks, although not to the extent of stiff networks, and resulted in intermediate levels of fibre/RGD recruitment (Fig. 5k). Cell proliferation in these soft welded networks was likewise intermediate between soft and stiff networks (Fig. 5l), supporting the model that fibre recruitment (and not the stiffness of individual fibres per se) is the primary mechanism of mechanotransduction observed in these studies.

Here, we describe a new biomaterial system that recapitulates the fibrous architecture of native ECMs while providing the control offered by synthetic materials. Using this material, we uncovered a previously unrecognized mechanism for transducing matrix stiffness, whereby lower fibre/network stiffness enabled cells to recruit nearby fibres, leading to increased local adhesive ligand density, enhanced adhesion signalling, cell spreading and proliferative signalling. Notably, we find that multiple structural parameters of fibre networks (that is, fibre stiffness, fibre–fibre welding and fibre density) converge through cellular fibre recruitment to influence cell function. This link between fibre recruitment and proliferation suggests that spatial rearrangements of ECM are not merely a consequence of cellular forces, but can also feedback to alter cell signalling and function[31]. Moreover, given that these pronounced structural rearrangements are absent in traditional elastic hydrogel materials, these findings highlight the need for new materials that can more accurately capture the mechanical behaviour of native ECMs. Recent work identifying a role for substrate stress relaxation in cell spreading through the introduction of viscoelasticity to gels further illustrates this need[47]. Future innovation to incorporate such properties in addition to dynamic features (that is, cell-mediated matrix degradation, synthesis and crosslinking) into fibrous materials will be critical in further refining our understanding of the feedback between matrix structure/mechanics and the cellular response.

Most tissues possess bulk moduli in the pascal to kilopascal range, whereas the protein fibres that compose these tissues are often in the megapascal to gigakilopascal range[48,49]. Our ability to not only recapitulate these features in our synthetic fibre networks, but also independently tune mechanics at different length scales may provide a path to elucidating how cells assimilate mechanical signals from multiple length scales (for example, through integrin clustering and focal adhesion assembly at the nanoscale[21,50] and through actomyosin activity between focal adhesions to probe stiffness at the microscale[51,52]). Integrating insights offered by such materials with theoretical approaches that couple the hierarchical structure and mechanics of fibrous ECM (refs 53,54) to models of intracellular dynamics (integrin engagement[39,50], stress fibre formation[55], focal adhesion assembly[56]) will be an essential and exciting step towards this goal.

Methods

Methods and any associated references are available in the online version of the paper.

Received 10 September 2014; accepted 28 August 2015; published online 12 October 2015

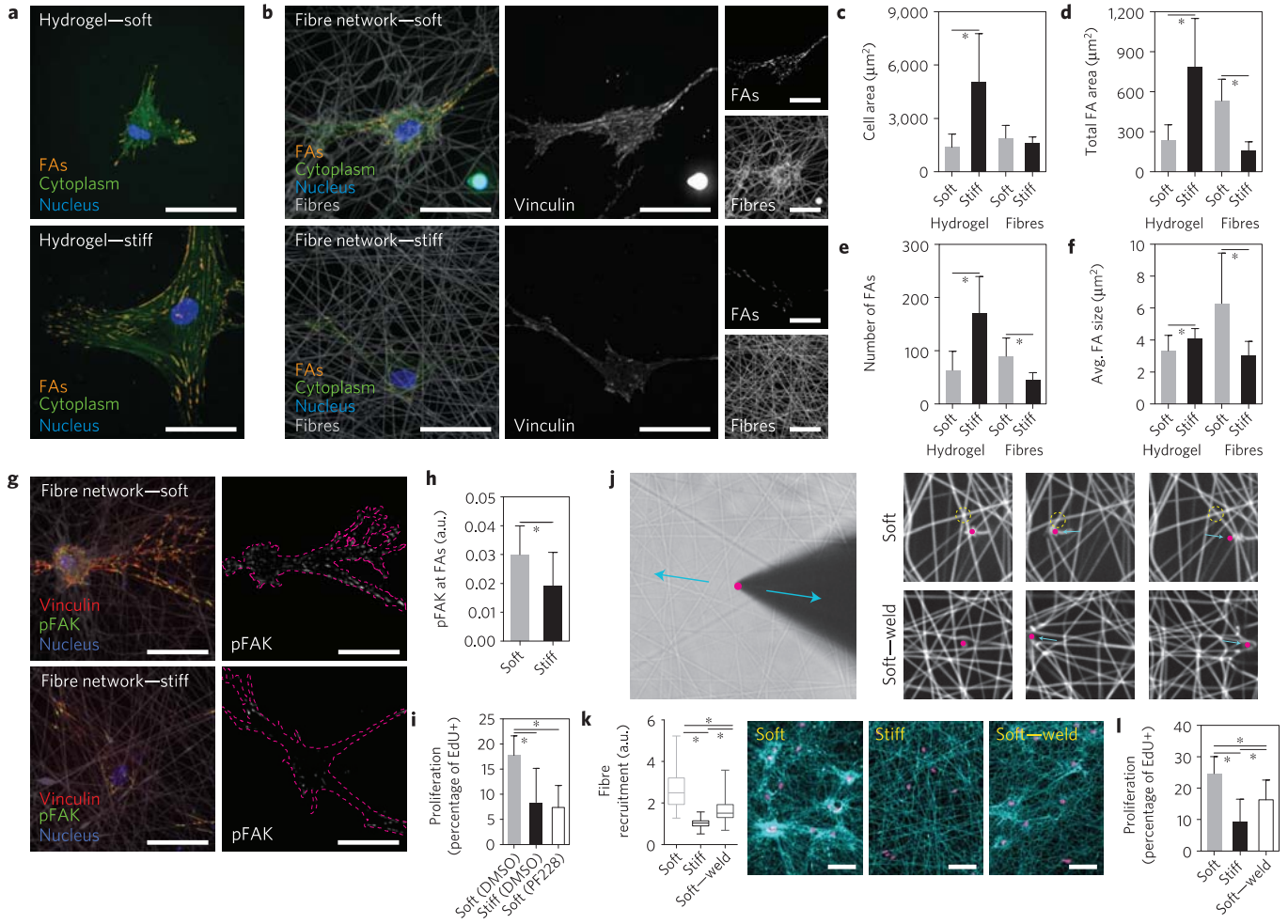

Figure 5 | Fibrillar ECM remodelling promotes FA formation and FAK phosphorylation to increase proliferation. a, FA formation of representative hMSCs seeded on DexMA hydrogels of low and high stiffness as visualized by cytosol extraction, vinculin immunostaining, and subsequent image analysis to identify FAs (orange). The cell's cytoplasm (green) and nucleus (blue) are also shown. Scale bars, 50 μm. **b**, FA formation of representative hMSCs on DexMA fibre networks of low and high fibre stiffness 16 h after seeding. Composite images (left) showing FAs (orange), cytoplasm (green), nuclei (blue) and fibres (grey). Single-channel images of vinculin (middle) and fibres (right, bottom) as well as identified FAs (right, top). Scale bars, 50 μm. **c–f**, Cell area (**c**), total FA area (**d**), total number of FAs (**e**), and average FA size (**f**); mean ± s.d., $n=12$ cells, $^*P<0.05$. **g**, Merged images of representative hMSCs 16 h after seeding co-stained for vinculin (red) and phospho-FAK (green). Single-channel images of phospho-FAK with cells outlined in magenta. Scale bars, 50 μm. **h**, Quantification of phospho-FAK localization to FAs determined by fluorescence intensity; mean ± s.d., $n=10$ cells, $^*P<0.05$. **i**, Effect of FAK phosphorylation inhibition on proliferation of hMSCs over 2 days, as determined by EdU incorporation; mean ± s.d., $n\geq 9$ ROI with totals of 450–1,500 cells analysed, $^*P<0.05$. **j**, To test fibre–fibre connectivity, a diamond-sharpened blade was placed adjacent to individual fibres and reciprocated using a micromanipulator. Blade tip position indicated with magenta circle; direction of translation indicated with cyan arrows. Soft networks as fabricated in all previous studies possess limited connectivity as demonstrated by free sliding of fibres (top row) in contrast to 'welded' networks with high fibre–fibre connectivity (bottom row). **k**, Remodelling of fibre networks 16 h after MSC seeding. Fibre recruitment in 50-μm-diameter circular regions centred on the cell nucleus. Fibres imaged by coupling with rhodamine methacrylate (cyan) and thresholded cell nuclei labelled with Hoechst 33342 (magenta). Scale bars, 100 μm. Fluorescence intensity was normalized to adjacent acellular areas. **l**, Effect of altering fibre–fibre connectivity on proliferation of hMSCs over 2 days as determined by EdU incorporation; mean ± s.d., $n\geq 9$ ROI with totals of 450–1,500 cells analysed, $^*P<0.05$.

References

1. Discher, D. E., Janmey, P. & Wang, Y. Tissue cells feel and respond to the stiffness of their substrate. *Science* **310,** 1139–1143 (2005).
2. Wozniak, M. A. & Chen, C. S. Mechanotransduction in development: A growing role for contractility. *Nature Rev. Mol. Cell Biol.* **10,** 34–43 (2009).
3. Jaalouk, D. E. & Lammerding, J. Mechanotransduction gone awry. *Nature Rev. Mol. Cell Biol.* **10,** 63–73 (2009).
4. Pelham, R. J. & Wang, Y. Cell locomotion and focal adhesions are regulated by substrate flexibility. *Proc. Natl Acad. Sci. USA* **94,** 13661–13665 (1997).
5. Yeung, T. *et al.* Effects of substrate stiffness on cell morphology, cytoskeletal structure, and adhesion. *Cell Motil. Cytoskeleton* **60,** 24–34 (2005).
6. Engler, A. J., Sen, S., Sweeney, H. L. & Discher, D. E. Matrix elasticity directs stem cell lineage specification. *Cell* **126,** 677–689 (2006).
7. Engler, A. *et al.* Substrate compliance versus ligand density in cell on gel responses. *Biophys. J.* **86,** 617–628 (2004).
8. Pedersen, J. A. & Swartz, M. A. Mechanobiology in the third dimension. *Ann. Biomed. Eng.* **33,** 1469–1490 (2005).
9. Pathak, A. & Kumar, S. Biophysical regulation of tumor cell invasion: Moving beyond matrix stiffness. *Integr. Biol.* **3,** 267–278 (2011).
10. Baker, B. M. & Chen, C. S. Deconstructing the third dimension—how 3D culture microenvironments alter cellular cues. *J. Cell Sci.* **125,** 3015–3024 (2012).
11. Van Dijk-Wolthuis, W. N. E. *et al.* Synthesis, characterization, and polymerization of glycidyl methacrylate derivatized dextran. *Macromolecules* **28,** 6317–6322 (1995).
12. Yang, L. *et al.* Micromechanical bending of single collagen fibrils using atomic force microscopy. *J. Biomed. Mater. Res.* **82A,** 160–168 (2007).
13. Kluge, D., Abraham, F., Schmidt, S., Schmidt, H.-W. & Fery, A. Nanomechanical properties of supramolecular self-assembled whiskers determined by AFM force mapping. *Langmuir* **26,** 3020–3023 (2010).

14. Guthold, M. *et al.* A comparison of the mechanical and structural properties of fibrin fibers with other protein fibers. *Cell Biochem. Biophys.* **49,** 165–181 (2007).
15. Trappmann, B. *et al.* Extracellular-matrix tethering regulates stem-cell fate. *Nature Mater.* **11,** 642–649 (2012).
16. Knight, C. G. *et al.* The collagen-binding A-domains of integrins α1β1 and α2β1 recognize the same specific amino acid sequence, GFOGER, in native (triple–helical) collagens. *J. Biol. Chem.* **275,** 35–40 (2000).
17. Konitsiotis, A. D. *et al.* Characterization of high affinity binding motifs for the discoidin domain receptor DDR2 in collagen. *J. Biol. Chem.* **283,** 6861–6868 (2008).
18. Zhong, C. *et al.* Rho-mediated contractility exposes a cryptic site in fibronectin and induces fibronectin matrix assembly. *J. Cell Biol.* **141,** 539–551 (1998).
19. Klotzsch, E. *et al.* Fibronectin forms the most extensible biological fibers displaying switchable force-exposed cryptic binding sites. *Proc. Natl Acad. Sci. USA* **106,** 18267–18272 (2009).
20. Grinnell, F., Ho, C.-H., Tamariz, E., Lee, D. J. & Skuta, G. Dendritic fibroblasts in three-dimensional collagen matrices. *Mol. Biol. Cell* **14,** 384–395 (2003).
21. Huebsch, N. *et al.* Harnessing traction-mediated manipulation of the cell/matrix interface to control stem-cell fate. *Nature Mater.* **9,** 518–526 (2010).
22. Khetan, S. *et al.* Degradation-mediated cellular traction directs stem cell fate in covalently crosslinked three-dimensional hydrogels. *Nature Mater.* **12,** 458–465 (2013).
23. Cukierman, E., Pankov, R., Stevens, D. R. & Yamada, K. M. Taking cell-matrix adhesions to the third dimension. *Science* **294,** 1708–1712 (2001).
24. Hakkinen, K. M., Harunaga, J. S., Doyle, A. D. & Yamada, K. M. Direct comparisons of the morphology, migration, cell adhesions, and actin cytoskeleton of fibroblasts in four different three-dimensional extracellular matrices. *Tissue Eng. Part A* **17,** 713–724 (2010).
25. Fraley, S. I. *et al.* A distinctive role for focal adhesion proteins in three-dimensional cell motility. *Nature Cell Biol.* **12,** 598–604 (2010).
26. Kubow, K. E. & Horwitz, A. R. Reducing background fluorescence reveals adhesions in 3D matrices. *Nature Cell Biol.* **13,** 5–7 (2011).
27. Stopak, D. & Harris, A. K. Connective tissue morphogenesis by fibroblast traction: I. Tissue culture observations. *Dev. Biol.* **90,** 383–398 (1982).
28. Ma, X. *et al.* Fibers in the extracellular matrix enable long-range stress transmission between cells. *Biophys. J.* **104,** 1410–1418 (2013).
29. Guo, C.-L. *et al.* Long-range mechanical force enables self-assembly of epithelial tubular patterns. *Proc. Natl Acad. Sci. USA* **109,** 5576–5582 (2012).
30. Shi, Q. *et al.* Rapid disorganization of mechanically interacting systems of mammary acini. *Proc. Natl Acad. Sci. USA* **111,** 658–663 (2014).
31. Provenzano, P. *et al.* Collagen reorganization at the tumor-stromal interface facilitates local invasion. *BMC Med.* **4,** 38 (2006).
32. Grinnell, F. & Lamke, C. R. Reorganization of hydrated collagen lattices by human skin fibroblasts. *J. Cell Sci.* **66,** 51–63 (1984).
33. Tomasek, J. J., Haaksma, C. J., Eddy, R. J. & Vaughan, M. B. Fibroblast contraction occurs on release of tension in attached collagen lattices: Dependency on an organized actin cytoskeleton and serum. *Anat. Rec.* **232,** 359–368 (1992).
34. Kolodney, M. S. & Elson, E. L. Correlation of myosin light chain phosphorylation with isometric contraction of fibroblasts. *J. Biol. Chem.* **268,** 23850–23855 (1993).
35. Mih, J. D., Marinkovic, A., Liu, F., Sharif, A. S. & Tschumperlin, D. J. Matrix stiffness reverses the effect of actomyosin tension on cell proliferation. *J. Cell Sci.* **125,** 5974–5983 (2012).
36. Wang, H.-B., Dembo, M. & Wang, Y.-L. Substrate flexibility regulates growth and apoptosis of normal but not transformed cells. *Am. J. Phys.* **279,** C1345–C1350 (2000).
37. Wang, L.-S., Boulaire, J., Chan, P. P. Y., Chung, J. E. & Kurisawa, M. The role of stiffness of gelatin–hydroxyphenylpropionic acid hydrogels formed by enzyme-mediated crosslinking on the differentiation of human mesenchymal stem cell. *Biomaterials* **31,** 8608–8616 (2010).
38. Cavalcanti-Adam, E. A. *et al.* Cell spreading and focal adhesion dynamics are regulated by spacing of integrin ligands. *Biophys. J.* **92,** 2964–2974 (2007).
39. Chan, C. E. & Odde, D. J. Traction dynamics of filopodia on compliant substrates. *Science* **322,** 1687–1691 (2008).
40. Yang, M. T., Sniadecki, N. J. & Chen, C. S. Geometric considerations of micro- to nanoscale elastomeric post arrays to study cellular traction forces. *Adv. Mater.* **19,** 3119–3123 (2007).
41. Balaban, N. Q. *et al.* Force and focal adhesion assembly: A close relationship studied using elastic micropatterned substrates. *Nature Cell Biol.* **3,** 466–472 (2001).
42. Chen, C. S., Alonso, J. L., Ostuni, E., Whitesides, G. M. & Ingber, D. E. Cell shape provides global control of focal adhesion assembly. *Biochem. Biophys. Res. Commun.* **307,** 355–361 (2003).
43. Pasapera, A. M., Schneider, I. C., Rericha, E., Schlaepfer, D. D. & Waterman, C. M. Myosin II activity regulates vinculin recruitment to focal adhesions through FAK-mediated paxillin phosphorylation. *J. Cell Biol.* **188,** 877–890 (2010).
44. Slack-Davis, J. K. *et al.* Cellular characterization of a novel focal adhesion kinase inhibitor. *J. Biol. Chem.* **282,** 14845–14852 (2007).
45. Houseman, B. T. & Mrksich, M. The microenvironment of immobilized Arg-Gly-Asp peptides is an important determinant of cell adhesion. *Biomaterials* **22,** 943–955 (2001).
46. Arnold, M. *et al.* Activation of integrin function by nanopatterned adhesive interfaces. *Chem. Phys. Chem.* **5,** 383–388 (2004).
47. Chaudhuri, O. *et al.* Substrate stress relaxation regulates cell spreading. *Nature Commun.* **6,** 6365 (2015).
48. Fratzl, P. *Collagen: Structure and Mechanics* (Springer Science and Business Media, 2008).
49. Gautieri, A., Vesentini, S., Redaelli, A. & Buehler, M. J. Hierarchical structure and nanomechanics of collagen microfibrils from the atomistic scale up. *Nano Lett.* **11,** 757–766 (2011).
50. Elosegui-Artola, A. *et al.* Rigidity sensing and adaptation through regulation of integrin types. *Nature Mater.* **13,** 631–637 (2014).
51. Choquet, D., Felsenfeld, D. P. & Sheetz, M. P. Extracellular matrix rigidity causes strengthening of integrin-cytoskeleton linkages. *Cell* **88,** 39–48 (1997).
52. Fu, J. *et al.* Mechanical regulation of cell function with geometrically modulated elastomeric substrates. *Nature Methods* **7,** 733–736 (2010).
53. Sander, E. A., Stylianopoulos, T., Tranquillo, R. T. & Barocas, V. H. Image-based multiscale modeling predicts tissue-level and network-level fiber reorganization in stretched cell-compacted collagen gels. *Proc. Natl Acad. Sci. USA* **106,** 17675–17680 (2009).
54. Abhilash, A. S., Baker, B. M., Trappmann, B., Chen, C. S. & Shenoy, V. B. Remodeling of fibrous extracellular matrices by contractile cells: Predictions from discrete fiber network simulations. *Biophys. J.* **107,** 1829–1840 (2014).
55. Walcott, S. & Sun, S. X. A mechanical model of actin stress fiber formation and substrate elasticity sensing in adherent cells. *Proc. Natl Acad. Sci. USA* **107,** 7757–7762 (2010).
56. Besser, A. & Safran, S. A. Force-induced adsorption and anisotropic growth of focal adhesions. *Biophys. J.* **90,** 3469–3484 (2006).

Acknowledgements

This work was supported in part by grants from the National Institutes of Health (grant numbers EB000262, EB001046, HL115553, GM74048, AR056624) and Center for Engineering Cells and Regeneration of the University of Pennsylvania. B.M.B. acknowledges financial support from a Ruth L. Kirschstein National Research Service Award (EB014691) and NIH Pathway to Independence Award (HL124322). We would like to thank N. Wang for helpful discussions. We would also like to acknowledge support from the Penn Regional Nanotechnology Facility and the BME Core Facilities at Boston University.

Author contributions

B.M.B., B.T., J.A.B. and C.S.C. designed the materials. B.M.B., B.T. and C.S.C. designed the experiments. B.M.B., B.T., W.Y.W., M.S.S. and I.L.K. conducted experiments and analysed data. V.B.S. helped with analysis and interpretation of mechanical testing data. B.M.B., B.T. and C.S.C. wrote the manuscript.

Additional information

Supplementary information is available in the online version of the paper. Reprints and permissions information is available online at www.nature.com/reprints. Correspondence and requests for materials should be addressed to B.M.B. or C.S.C.

Competing financial interests

The authors declare no competing financial interests.

Methods

All reagents were from Sigma-Aldrich and were used as received, unless otherwise stated.

Synthesis of methacrylated dextran (DexMA). Dextran (MP Biomedicals, MW 86,000 kDa) was methacrylated by reaction with glycidyl methacrylate, according to a modified, previously described procedure[11]. In brief, dextran (20 g) and 4-dimethylaminopyridine (2 g) were dissolved in anhydrous dimethylsulphoxide (100 ml) under vigorous stirring. Glycidyl methacrylate (24.6 ml) was added and the reaction mixture was heated to 45 °C for 24 h. The solution was cooled on ice for 20 min and precipitated into 1 l ice-cold 2-isopropanol. The crude product was recovered by centrifugation, redissolved in milli-Q water and dialysed against milli-Q water for 3 days. The final product was lyophilized and stored at −20 °C until use. DexMA was characterized by ^{1}H-NMR (Supplementary Fig. 1). The degree of functionalization was calculated as the ratio of the averaged methacrylate proton integral (6.174 ppm and 5.713 ppm in D_2O) and the anomeric proton of the glycopyranosyl ring (5.166 ppm and 4.923 ppm). As the signal of the anomeric proton of α-1,3 linkages (5.166 ppm) partially overlaps with other protons, a pre-determined ratio[11] of 4% α-1,3 linkages was assumed and the total anomeric proton integral was calculated solely on the basis of the integral at 4.923 ppm. A methacrylate/dextran repeat unit ratio of 0.7 was determined.

DexMA fibre network fabrication. Three-dimensional networks of suspended DexMA fibres were fabricated by a combination of electrospinning and standard soft photolithography. DexMA was dissolved at 0.3–0.6 g ml^{-1} in a 1:1 mixture of milli-Q water and dimethylformamide with 0.005% Irgacure 2959 photoinitiator (Ciba). Electrospinning was accomplished with a custom set-up consisting of a high-voltage power supply (Gamma High Voltage Research), syringe pump (KD Scientific), and grounded copper or aluminium collecting surface enclosed within an environmental chamber (Terra Universal). Electrospinning was performed at a flow rate of 0.5 ml h^{-1}, voltage of 7.5 kV, and gap distance of 8 cm (Supplementary Fig. 11a,b) To induce a preferred direction of fibre alignment (Fig. 1), the static grounded surface (6 × 6 × 1/8 inch copper sheet) was replaced with a motorized platen rotating at 1,200 r.p.m., a speed sufficient to translate the substrate at a linear velocity of 10 m s^{-1} (Supplementary Fig. 11c,d). Samples were primary crosslinked under ultraviolet light to stabilize fibres, hydrated in a solution containing 1 mg ml^{-1} Irgacure 2959, and then exposed to varying durations of ultraviolet light (100 mW cm^{-2}) to control the degree of crosslinking and resulting stiffness. Fibres were collected on poly(dimethylsiloxane) (PDMS; Sylgard 184, Dow-Corning, Midland) arrays of circular wells (2 mm diameter) functionalized with methacrylates to promote fibre adhesion. Briefly, silicon wafer masters possessing SU-8 photoresist (Microchem) were produced by standard photolithography and used to generate PDMS stamps. Following silanization with trichloro(1H,1H,2H,2H-perfluorooctyl)silane, stamps were used to emboss uncured PDMS onto oxygen plasma-treated coverslips. Well arrays were methacrylated with a 2% v/v solution of 3-(trimethoxysilyl)propyl methacrylate in ethanol for at least 24 h. To promote fibre–fibre welding, fibre networks were briefly exposed to a humidified environment (60% relative humidity, determined empirically) before primary crosslinking. This approach to fuse fibres at overlaying intersection points was predicated on previous work showing the influence of solvent volatility on fibre–fibre welding[57]. Lateral displacements using a diamond dissecting knife (Type MDL, Electron Microscopy Sciences) controlled by a micromanipulator (HCU-3DM, SmarAct GMBH) were applied to networks to confirm the introduction of fibre–fibre welding.

DexMA hydrogel preparation. DexMA was dissolved at 3.75% w/v in M199 medium containing sodium bicarbonate (3.5% w/v) and HEPES (10 mM). Irgacure 2959 in ethanol (10 mg ml^{-1}) was added to a final concentration of 0.02% w/v. Solutions were mixed and spread onto methacrylated coverslips (below). Hydrogel precursors were photopolymerized using an Omnicure S2000 UV lamp (EXFO) at 100 mW cm^{-2} (measured at 365 nm). Polymerization times were 7.5 s for soft and 30 s for intermediate-stiffness hydrogels. Stiff hydrogels were polymerized for 60 s in an argon chamber. To functionalize coverslips with methacrylates, No. 1 thickness, borosilicate glass coverslips were plasma oxidized using air plasma (K1050X, Emitech) and immersed in a 2% v/v solution of 3-(trimethoxysilyl)propyl methacrylate in anhydrous toluene for at least 24 h. Before use, coverslips were washed in ethanol and water and dried under a stream of nitrogen.

Collagen matrices. Solutions of rat tail collagen I (BD Biosciences) at various concentrations were prepared as in ref. 58 and pipetted onto glutaraldehyde-functionalized glass coverslips. Coverslips were prepared by exposure to oxygen plasma and immediate treatment with sequential 2 h incubations in 0.1 mg ml^{-1} poly-L-lysine and 5% v/v glutaraldehyde.

Mechanical testing. To determine the tensile mechanical properties of individual fibres, three-point bending tests were performed using atomic force microscopy (AFM). Single fibres were collected on 200 μm wide by 200 μm tall microfabricated PDMS troughs by electrospinning for short durations (1–3 s). Fibres were hydrated and crosslinked to varying degrees by ultraviolet light exposure as above, and deformed by an AFM tip (0.06 N m^{-1}) loaded with a 25-μm-diameter bead positioned centrally along the fibre's length. Young's modulus was calculated from the resulting load–displacement curves using known equations for a cylindrical rod undergoing three-point bending with fixed boundaries (confirmed experimentally, Supplementary Fig. 2). This measurement was performed on a population basis, using a mean fibre diameter to calculate Young's modulus from the same population's mean stiffness. For flat hydrogels, AFM nanoindentation testing was performed with the same probe as above. Young's modulus was determined by fitting force-indentation curves to known models for Hertzian contact of a spherical indentor on an elastic half-space, assuming a Poisson ratio of 0.5. Mechanical properties of fibrous networks as fabricated for cell studies were determined by indentation with a rigid cylinder. Cylinders (500 μm diameter, 500 μm tall) of SU8 photoresist were microfabricated and affixed to pure tungsten filaments of known mechanical properties. Indentation was performed with a micromanipulator, using a confocal microscope to determine the resulting plane of the fibres at each step of indentation. Young's modulus was approximated assuming an elastic membrane using the following equation,

$$F = \frac{Et\pi\delta^3(r_o^2 - r_i^2)}{2(r_o - r_i)^4(1-\nu)}$$

where t is the membrane thickness (20 μm), r_o is the membrane diameter (1 mm), r_i is the indentor diameter (0.25 mm), and ν is the Poisson ratio (0.5), F is the indentation force, δ is the indentation depth, and E is Young's modulus.

RGD functionalization of DexMA fibre networks and hydrogels. For cell studies, DexMA fibre networks and hydrogels were functionalized with the cell-adhesive peptide CGRGDS, custom synthesized by Aapptec and supplied as a trifluoroacetate salt. A CGRGDS concentration of 2 mM was used for most cell studies. To couple CGRGDS to available methacrylates using Michael addition, the peptide was dissolved in M199 medium containing sodium bicarbonate (3.5% w/v) and HEPES (10 mM) and 1 M NaOH (about 10 μl ml^{-1} solution) was added to adjust the pH to 7.5–8. The solution was transferred to the substrates and incubated for 1 h at room temperature. Following functionalization, substrates were thoroughly rinsed with PBS before cell seeding. In additional studies, quantifying the amount of CGRGDS on fibre substrates, peptides were fluorescently labelled with FITC. CGRGDS (100 mg) was dissolved in 0.15 M sodium bicarbonate buffer (700 μl), the solution was adjusted to pH 8 using 1 M sodium hydroxide, and a solution of fluorescein-*N*-hydroxysuccinimide (Fisher Scientific) in dimethylsulphoxide (100 mg in 300 μl) was introduced. The mixture was allowed to react for 3 h at room temperature on a shaker. It is noted that *N*-hydroxysuccinimide will partially precipitate in aqueous buffer, but will redissolve on reaction within the first hour of addition. The reaction mixture was desalted using a PD-10 column (Life Technologies) and lyophilized.

Cell culture. NIH 3T3 fibroblasts were cultured in high-glucose DMEM containing 1% penicillin/streptomycin, L-glutamine, and 10% bovine serum. Human MSCs were cultured in low-glucose DMEM containing 1% penicillin/streptomycin, and 10% fetal bovine serum (basal media) and expanded to between passage 4 and 6 before use. In typical studies, substrates were seeded at 2,000 cells cm^{-2} and maintained in basal media. For studies requiring multicellular clusters, pyramid-shaped microwells (AggreWell, Stemcell Technologies) were used to generate spheroids containing 1,000 MSCs. For contraction assays, MSCs were seeded at 10,000 cells cm^{-2}. For studies requiring the inhibition of FAK phosphorylation, PF 573228 (Tocris Biosciences) was added to basal medium at a concentration of 1 μM.

Fluorescent staining and microscopy. MSCs on fibre and hydrogel substrates were fixed in 4% paraformaldehyde for 15 min at room temperature. Alternatively, to extract cytoplasmic vinculin, samples were simultaneously fixed and permeabilized in 2% paraformaldehyde in microtubule-stabilizing buffer for 15 min at room temperature. To examine the organization of the actin cytoskeleton, cells were permeabilized with Triton X-100, blocked in 2% BSA, and stained with phalloidin. For immunostaining, samples were permeabilized, blocked for 1 h in 10% fetal bovine serum containing 0.2% Tween, and incubated with primary (vinculin: 1:500 mouse monoclonal anti-vinculin (Sigma, V9264), phoshoFAK: 1:500 rabbit polyclonal anti-FAK (phospho Y397) (AbCam, ab39967)) and secondary (1:1,000 Alexa Fluor 488 goat anti-mouse IgG (H+L) or 1:1,000 Alexa Fluor 488 donkey anti-rabbit IgG (H+L) (Life Technologies)) consecutively for 1 h each at room temperature. For proliferation studies, EdU labelling was performed following the manufacturer's protocol (ClickIT EdU, Life Technologies). To quantify cell death within fibrous networks, staining with calcein AM/ethidium homodimer (LIVE/DEAD Cell Viability Assay, Life Technologies) was performed. High-resolution confocal imaging of phalloidin-stained samples was performed to

identify multinucleated cells, and did not reveal any evidence of incomplete cytokinesis. Samples were imaged at ×10 or 40 on a Zeiss 200M with a spinning-disc head (Yokogawa CSU-10 with Borealis), an environmental chamber, four laser lines, and a Photometric Evolve EMCCD camera. Unless otherwise specified, images are presented as maximum intensity projections. Cell area, proliferation, focal adhesion and fibre recruitment analyses were performed with custom Matlab scripts.

Statistics. Statistical differences were determined by analysis of variance or Student's t-test where appropriate, with significance indicated by $p < 0.05$. Sample size is indicated within corresponding figure legends. All data are presented as a mean ± s.d.

References

57. Kidoaki, S., Kwon, I. K. & Matsuda, T. Structural features and mechanical properties of *in situ*-bonded meshes of segmented polyurethane electrospun from mixed solvents. *J. Biomed. Mater. Res.* **76B,** 219–229 (2006).
58. Kuntz, R. M. & Saltzman, W. M. Neutrophil motility in extracellular matrix gels: Mesh size and adhesion affect speed of migration. *Biophys. J.* **72,** 1472–1480 (1997).